Journal of Magnetic Resonance **146,** 375–378 (2000)
doi:10.1006/jmre.2000.2175, available online at http://www.idealibrary.com on IDEAL®

Multifrequency EPR Spectra of Molecular Oxygen in Solid Air

Luca A. Pardi,* J. Krzystek,† Joshua Telser,‡ and Louis-Claude Brunel†

*Istituto di Fisica Atomica e Molecolare, National Research Council, S. Cataldo, 56100 Pisa, Italy; †National High Magnetic Field Laboratory, Florida State University, Tallahassee, Florida 32310; and ‡Chemistry Program, Roosevelt University, Chicago, Illinois 60605-1394

Received May 25, 2000; revised July 24, 2000

Multifrequency EPR spectra in the 94 to 550 GHz range were performed on solid air samples condensed at 5 K in the waveguide of a single pass probe. The spectra of molecular oxygen were observed and interpreted in the frame of the spin Hamiltonian model as axial $S = 1$ spectra with a zero field splitting parameter $D = 3.572(3)$ cm^{-1}. The result of this study is relevant in the field of high field–high frequency EPR application in which solid air O_2 is a common paramagnetic impurity. © 2000 Academic Press

Key Words: **EPR; high-field; molecular oxygen; triplet; zero field splitting.**

Molecular oxygen (O_2) is a paramagnetic molecule with a $^3\Sigma_g^-$ ground state. Gas phase EPR studies on the ground state of O_2, as well as on other paramagnetic molecules in the gas phase, date back to the 1950s (*1–5*). The gas phase EPR spectrum of O_2 is fairly complicated due to the coupling of orbital angular momentum **L**, spin angular momentum **S**, and the rigid body angular momentum of the molecule **N**. The spectrum shows a fine structure in which the dipolar spin–spin and spin–orbit components play the major role (*6*).

In condensed phases, however, the molecular rotations are efficiently quenched and the EPR properties of O_2 change accordingly. EPR spectra of O_2 have been observed at low temperature in nitrogen and in CO_2 matrices at both X- and Q-band microwave frequencies (*7*). The signals arising from O_2 that are observed using X-band EPR at low temperature can indeed be attributed to an $S = 1$ species with large zero field splitting (zfs), but these triplet spectra are obviously incomplete as they show only one component (see below). Moreover, at higher concentration the X-band spectrum broadens beyond observability. EPR spectra were also observed at 4 and 8 mm (75 and 37.5 GHz, respectively) in low-temperature experiments on O_2 trapped in β-quinol. The spectra of oxygen in these clathrate crystals were interpreted in the frame of a hindered rotation model (*8*).

With the development of high frequency–high field EPR spectroscopy (HF^2-EPR, >95 GHz) (*9–16*), informal reports of the observation of signals from molecular oxygen arising from condensed air in low-temperature experiments have become common, but no systematic study of these signals has been attempted. This contribution is intended to fill this void, by presenting a multifrequency, low-temperature study of the HF^2-EPR spectra that are due to O_2 in condensed air. We believe that this study will therefore be of utility to the expanding HF^2-EPR community, for whom molecular oxygen is mainly an undesired impurity.

The simplest way one can "prepare" the sample investigated in this work is either to decrease the temperature in the sample chamber without evacuating and/or flushing it with helium gas, or by freezing a sample solution contaminated with atmospheric oxygen. Another reported case in which air–O_2 signals occur is when there is a cold leak in the variable temperature apparatus. The amount of molecular oxygen that can be condensed is quite significant, as shown by a simple calculation. Many EPR spectrometers in use at millimeter and submillimeter wavelengths are implemented with probeheads using metallic circular oversized waveguides. If one takes a 1-m section of a typical waveguide with an inner diameter of 10 mm and assumes that the air contained in it at room temperature condenses at 4.2 K, then this volume of oxygen amounts to 7×10^{-4} mol; that is to say 4×10^{20} spins. Even condensing a volume of air six orders of magnitude smaller and taking into account the distribution of the EPR intensity over the fine structure of the spectrum, one would still have a number of spins per gauss that is observable even in low sensitivity experiments. It is thus clear how molecular oxygen can become a very common impurity in HF^2-EPR whenever the radiation used has a radiation quantum that is comparable to or larger than the observed zfs of the system. We report here the HF^2-EPR spectra of the air mixture that condenses at temperatures lower than 75 K in the transmission probe in use at the NHMFL. The spectrometer itself has been described previously (*16*). For comparison, the spectra reported in reference (*7*) were obtained at low temperature in a nitrogen matrix at an O_2 concentration ranging from 30 ppm to ~1% by volume. In the condensed air samples we are concerned with, the O_2 concentration is thus up to several orders of magnitude higher.

At temperatures lower than ~54 K the air sample is solid. The pure solid O_2 antiferromagnetically ordered phases (α- and β-O_2) (*17*), if present, could be observed by multifrequency antiferromagnetic resonance experiments (*18*). But in our samples the oxygen molecules are dispersed in the solid nitrogen

1090-7807/00 $35.00

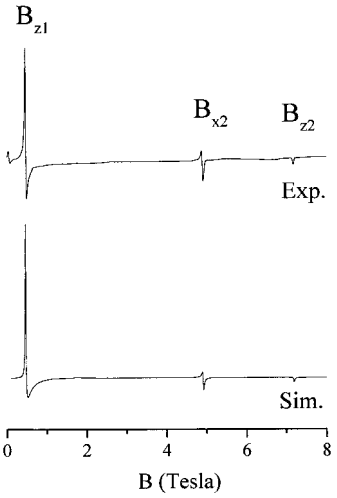

FIG. 1. 94.00 GHz EPR spectrum of O_2 in solid air at 5 K. Top, experimental; bottom, simulation. Experimental conditions: field sweep rate, 0.1 T/min; field modulation frequency, 8 kHz; modulation amplitude, 1.5 mT; lock-in time constant, 0.3 s. Simulation parameters, $S = 1$ with $D = 3.572$ cm^{-1} and $g = 2.000$; single-crystal linewidths used in the powder spectrum calculation, 20 mT (perpendicular peaks) and 10 mT (parallel peaks).

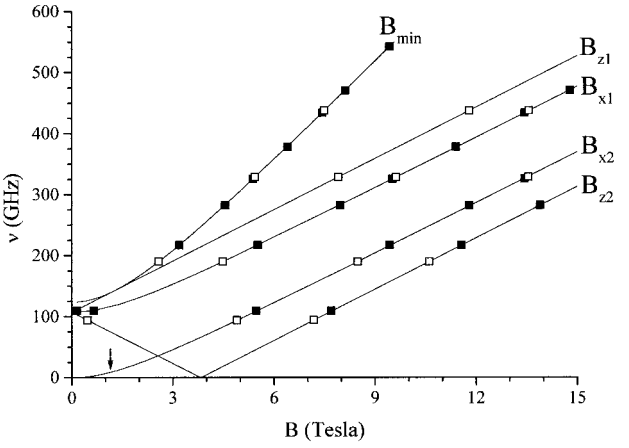

FIG. 3. Frequency versus magnetic field plot of the transition fields observed in the HF^2–EPR spectra of O_2 in solid air in the 94–550 GHz frequency range. The squares are experimental points: empty squares indicate the high precision data used in the fitting procedure (see text). The lines are calculated for a triplet state with $D = 3.572(3)$ cm^{-1} and $g = 2.000$. The arrow represents the feature observed in Ref. (*7*).

matrix and behave as ideal $S = 1$ paramagnets. These give rise to the typical triplet powder-pattern spectra as shown in Figs. 1 and 2 for 94 and 328 GHz, respectively. The HF^2-EPR spectrum of the same sample over the entire 94 to 550 GHz frequency range is reported in Fig. 3 in the form of a frequency versus resonant transition field plot. The specific locations of the transitions in Fig. 3 will be of assistance to workers in the HF^2-EPR area when confronted with cases where there is ambiguity about whether a given signal is due to a triplet (or higher multiplet) spin state of interest (*19, 20*), or simply due to O_2 contaminant.

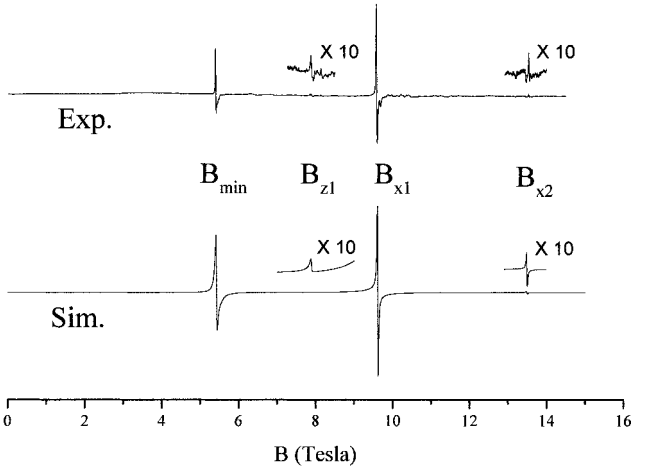

FIG. 2. 328.00 GHz EPR spectrum of O_2 in solid air at 5 K. Top, experimental; bottom, simulation. Experimental conditions as in legend to Fig. 1. Simulation parameters as in legend to Fig. 1 except for the single-crystal linewidths which were fixed at 20 mT (perpendicular peaks) and 5 mT (parallel peaks). The amplitude of the features labeled B_{z1} and B_{x2} in the observed and the calculated spectra were multiplied by a factor 10.

The interpretation of the multifrequency spectra is straightforward using a spin Hamiltonian of the form

$$H = g\mu_B B S_z + D\left(S_z^2 - \frac{S(S+1)}{3}\right). \qquad [1]$$

The transitions fields reported in Fig. 3 were fitted using Wasserman's equations (*21*), with our own program which performs a nonlinear regression based on the Levenberg–Marquardt method (*20*). The result of the fitting procedure for each particular transition among the triplet sublevels is shown as a continuous line in Fig. 3. The fitting procedure converged with $R = 2 \times 10^{-7}$ for a D value of 3.572(3) cm^{-1}, while fixing the g value isotropic and equal to 2.000. Attempts to fit the data by allowing the g values to vary did not improve the fit. The error in D is mainly determined by the experimental uncertainty in the observed transition fields, which in turn depends on the sweep rate and linearity of the magnetic field and on the linewidth. Only those data that were taken at low sweep rate (0.1 T/min), and thus with high accuracy, were used in the fitting procedure. These data amount to 14 of the 36 transition fields reported in Fig. 3 and are indicated in this figure as open squares. Simulations (*22*) of the spectra at 94 and 328 GHz at 5 K with the calculated spin Hamiltonian parameters as above are shown in Figs. 1 and 2, respectively. In these figures the transitions are labeled according to Wasserman (*21*); B_{z1} corresponds to the parallel transition $|S = 1, M_s = 0\rangle \rightarrow |1, +1\rangle$ and B_{z2} to $|1, 0\rangle \rightarrow |1, -1\rangle$, B_{min} is the off-axis turning point of the $\Delta M_s = \pm 2$ transition, while B_{x1} and B_{x2} are the perpendicular transitions. Minor discrepancies between the calculated

and observed relative amplitudes in Figs. 1 and 2 can be due either to slight temperature fluctuations of the sample during the sweep or to incomplete characterization of the linewidth anisotropy in the simulations. The weak signal at very low field present only in the experimental spectrum at 94 GHz is unidentified. Resonance field variations on the order of 50 mT were observed in these EPR spectra upon an increase from 5 to 10 K and the signal intensity decreases as well. These spectral variations can be due to a temperature dependence of the zfs as observed in different species (*23*). For this reason it must be stressed that the above fit parameters are those of the system at 5 K. A complete investigation of the temperature dependence of the spectrum is beyond the scope of this Communication.

These results from dilute, solid phase O_2 can be compared to those from gas phase spectra and to those in solid matrices (*7*). The fine structure parameter D is in all cases the sum of two contributions: the spin–spin dipolar contribution and the spin–orbit contribution. These two contributions cannot be disentangled within the spin Hamiltonian model where the different interactions are treated parametrically. As far as the gas phase spectrum is concerned, the zfs can be represented as an effective spin Hamiltonian for the free molecule that, considering the molecular rotations negligible, is given by (*2*)

$$H = \frac{2}{3}(\lambda_0 + \lambda_1\xi + \lambda_2\xi^2)(3S_z^2 - S^2), \qquad [2]$$

where the fine structure parameter D is expressed as an expansion in the variable ξ, which is defined in terms of the equilibrium and instantaneous internuclear distances, respectively, R_0 and R, as $\xi = (R - R_0)/R_0$. The λ_i terms in Eq. [2] are treated simply as fit parameters; to give them a physical meaning it is necessary to address more sophisticated theoretical tools than those provided by the spin Hamiltonian model (*2*). In the solid, ξ is expected to be small; thus from Eqs. [1] and [2], the zfs splitting parameter D arises only from λ_0. From the gas phase spectra (*1, 2*), $D = 2\lambda_0 = 3.96\ \text{cm}^{-1}$, as opposed to the value of $3.572\ \text{cm}^{-1}$ found here. It must be noted, however, that the gas phase spectra were recorded at room and to liquid nitrogen temperatures on a pure low-pressure oxygen gas sample. Therefore it is difficult to compare these two cases. A more meaningful comparison can be made with the experiment performed on a 30 ppm mixture of O_2 in nitrogen at 8.928 GHz and 6.8 K, although the spectra were incomplete due to field limitations and show a single feature, centered at 1.1465 T, arising from a turning point in the powder pattern (*7*). The calculated resonance field for a perpendicular transition of a triplet of $D = 3.572\ \text{cm}^{-1}$ at 8.928 GHz is 1.1497(30) Tesla. This transition is labeled B_{x2} in our model as shown in Fig. 3 where the position of this feature has been indicated by an arrow. Taking into account the experimental error, the slight temperature difference, and the fact that the zfs is influenced both by the nature of the matrix and by the oxygen concentration (*5*), we can consider the agreement quite satisfactory in this case. A comparison should be also made with the EPR spectra of O_2 molecules trapped in β-quinol clathrate (*8*). In the crystal β-quinol contains nearly spherical cages which can properly accommodate a variety of gas molecules. The low-temperature EPR spectra of trapped molecular oxygen, recorded at 75 and 38 GHz, can be interpreted in the frame of a hindered rotation model in which the hindrance to rotation is described by an appropriate potential function (*8*). When the potential is infinite, that is when the molecular axis is fixed, the zfs parameter D equals $3.93\ \text{cm}^{-1}$. The effect of partially hindered rotation is the reduction of the zfs parameter from this value to the observed value of $3.03\ \text{cm}^{-1}$. According to this model it is apparent that for O_2 in solid air and in other solid matrices, the hindrance to rotation is more effective than in the case of the β-quinol clathrate. The close resemblance between the fixed axis value of the zfs parameter for the trapped molecule ($3.93\ \text{cm}^{-1}$) and that reported for the gas phase molecule ($3.96\ \text{cm}^{-1}$) must be fortuitous. It may be of some interest in molecular physics to repeat the experiments of references (*1, 7, 8*) at the high frequencies and fields now available in a number of laboratories.

ACKNOWLEDGMENTS

J.T. thanks Roosevelt University and the NHMFL User Program for financial support. L.A.P. thanks the Consorzio INSTM for financial support. We acknowledge Dr. Høgni Weihe from the H. C. Ørsted Institute in Copenhagen, Denmark, for the simulation software.

REFERENCES

1. M. Tinkham and M. W. P. Strandberg, Interaction of molecular oxygen with a magnetic field, *Phys. Rev.* **97,** 951–966 (1955).
2. M. Tinkham and M. W. P. Strandberg, Theory of the fine structure of the molecular oxygen ground state, *Phys. Rev.* **97,** 937–950 (1955).
3. H. Levy, Gas phase magnetic resonance of electronically excited molecules, *Adv. Magn. Reson.* **6,** 1–71 (1973).
4. W. Weltner, Jr., "Magnetic Atoms and Molecules," Chap. III, Dover Publications, New York (1983).
5. G. R. Smith and W. Weltner, Jr., ESR of the triplet molecules CCO and CNN in rare-gas matrices; isotope and matrix effects, *J. Chem. Phys.* **62,** 4592–4604 (1975).
6. S. R. Langhoff, Ab initio evaluation of the fine structure of the oxygen molecule, *J. Chem. Phys.* **61,** 1708–1716 (1974).
7. Kon, Paramagnetic resonance of molecular oxygen in condensed phases, *J. Am. Chem. Soc.* **95,** 1045–1049 (1973).
8. S. Foner, H. Meyer, and W. H. Kleiner, Low temperature paramagnetic resonance of trapped O_2, *J. Phys. Chem. Solids* **18,** 273–285 (1961).
9. G. R. Eaton and S. S. Eaton, High-field and high-frequency EPR, *Appl. Magn. Reson.* **16,** 161–166 (1999).
10. L. Barra, L. C. Brunel, D. Gatteschi, L. Pardi, and R. Sessoli, High-frequency EPR spectroscopy of large metal ion clusters: From zero field splitting to quantum tunneling of the magnetization, *Acc. Chem. Res.* **31,** 460–466 (1998).
11. W. R. Hagen, High frequency EPR of transition ion complexes and metalloproteins. *Coord. Chem. Rev.* **190–192,** 209–229 (1999).

12. K. A. Earle and J. H. Freed, Quasioptical hardware for a flexible FIR-EPR spectrometer, *Appl. Magn. Reson.* **16,** 247–272 (1999).
13. A. Bloess, K. Mobius, and T. F. Prisner, High-frequency/high-field electron spin echo envelope modulation study of nitrogen hyperfine and quadrupole interactions on a disordered powder sample, *J. Magn. Reson.* **134,** 30–35 (1998).
14. Ya. S. Lebedev, Very-high-field EPR and its applications, *Appl. Magn. Reson.* **7,** 339–362 (1994).
15. S. Kimura, H. Ohta, M. Motokawa, T. Yokoo, and J. Akimitsu, ESR study of haldane system Y_2BaNiO_5 in submillimeter wave region, *J. Magn. Magn. Mater.* **177,** 624–625 (1998).
16. Hassan, L. A. Pardi, J. Krzystek, A. Sienkiewicz, P. Goy, M. Rohrer, and L. C. Brunel, Ultrawide band multifrequency high-field EMR technique: A methodology for increasing spectroscopic information, *J. Magn. Reson.* **142,** 300–312 (2000).
17. In the liquid and solid state the magnetic properties of pure molecular oxygen are "spin only" in nature. At room pressure pure oxygen solidifies at 48 K to form the γ phase ($\gamma - O_2$). The susceptibility of the liquid and of $\gamma - O_2$ obey the Curie Weiss law, $\chi(T) + \theta =$ constant, with a negative value of θ. Concerning the other two solid phases, $\beta - O_2$ is the phase stable below 43.8 K and shows antiferromagnetic behavior with no transition to a magnetically ordered phase, and $\alpha - O_2$, the phase stable below 23.886 K, is antiferromagnetically ordered at 4 K. This information was taken from E. A. V. Ebsworth, J. A. Connor, and J. J Turner *in* "Comprehensive Inorganic Chemistry" (J. C. Bailar, H. J. Emeleus, R. Nyholm, A. F. Trotman Dickinson, Eds.), Vol. 2, pp. 685–709. Pergamon Press, Oxford (1973).
18. G. E. Fanucci, J. Krzystek, M. W. Meisel, L. C. Brunel, and D. R. Talham, Antiferromagnetic resonance as a tool for investigating magnetostructural correlations: The canted antiferromagnetic state of $KMnPO_4$ H_2O and a series of manganese phosphonates, *J. Am. Chem. Soc.* **120,** 5469–5479 (1998).
19. H. R. Jimenez, J. Salgado, J. M. Moratal, and I. Morgenstern-Badarau, EPR and magnetic susceptibility studies of cobalt(II)- and nickel(II)-substituted azurins from *Pseudomonas aeruginosa.* Electronic structure of the active sites, *Inorg. Chem.* **35,** 2737–2741 (1996).
20. L. A. Pardi, A. K. Hassan, F. B. Hulsbergen, J. Reedijk, A. L. Spek, and L. C. Brunel, Direct determination of the single-ion anisotropy in a one-dimensional magnetic system by high-field EPR spectroscopy; Synthesis, EPR, and X-ray structure of $Ni_xZn_{1-x}(C_2O_4)(DMIz)_2$ [$X = 0.07$], *Inorg. Chem.* **39,** 159–164 (2000).
21. E. Wasserman, L. C. Snyder, and W. A. Yager, ESR of the triplet states of randomly oriented molecules, *J. Chem. Phys.* **41,** 1763–1772 (1964).
22. J. Glerup and H. Weihe, Magnetic susceptibility and EPR spectra of μ-cyano-bis[pentaammine-chromium(III)]Perchlorate, *Acta Chem. Scand.,* 444 (1991): The simulation software package is freely distributed by Dr. H. Weihe; for more information see the WWW page: http://sophus.kiku.dk/epr/epr.html.
23. S. Rubins, J. D. Clark, and S. K. Jani, Electron paramagnetic resonance in nickel fluosilicate, *J. Chem. Phys.* **67,** 893–896 (1977).